

Fractional order PID controller design of a DC-DC multilevel boost converter using the Nelder-Mead optimization

Ghrissi Tahri^{1,2}, Fatima Tahri^{3,2}, Ali Tahri²

¹Institut des Sciences et Techniques Appliquées (ISTA), Université Oran 1 Ahmed Ben Bella, Oran, Algeria

²Laboratoire de Génie Electrique d'Oran (LGEO), Department of Electrotechnics, Faculty of Electrical Engineering, University of Sciences and Technology of Oran Mohamed Boudiaf, Oran, Algeria

³Laboratoire de Développement des Réseaux Electriques Intelligents (LDREI), Ecole Supérieure en Génie Electrique et Energétique d'Oran (ESGEE), Oran, Algeria

Article Info

Article history:

Received Feb 9, 2024

Revised Jun 27, 2024

Accepted Jul 24, 2024

Keywords:

DC-DC 2-L MBC

Fractional order PID

Fuzzy logic control

Nelder-Mead optimization

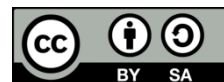
algorithm

Stat space averaging

ABSTRACT

This paper aims to present and analyze the fractional order proportional-integral-derivative (FOPID) control technique of the DC-DC two-level boost converter. The state-space averaged (SSA) method is used to build a small-signal converter mathematical model, which is a crucial task for the control design. A FOPID controller based on the Nelder-Mead optimization algorithm and an artificial intelligence strategy based on a fuzzy logic controller (FLC) are both designed for the voltage mode control (VMC) approach and operate on the continuous conduction mode (CCM). Various step changes in the input voltage amplitude and output load are applied to analyze the performance of the proposed control techniques. In addition, detailed simulation results using the MATLAB-Simulink system are extensively discussed.

This is an open access article under the [CC BY-SA](#) license.



Corresponding Author:

Ghrissi Tahri

Institut des Sciences et Techniques Appliquées (ISTA), Université Oran 1 Ahmed Ben Bella

Oran, Algeria

Email: tahri.ghrissi@univ-oran1.dz, ghrissi.tahri@univ-usto.dz

1. INTRODUCTION

The fuzzy logic control system which is based on human expertise was introduced in 1975 by Mamdani and Assilian. It was implemented as an experiment on linguistic controller synthesis for a steam engine-based model industrial plant [1]. Moreover, since 1989, fuzzy logic control has been used in many domestic electric appliances. Fuzzy logic allows such appliances to be accurate and straightforward in dealing with qualitative knowledge of operations, which are described as fuzzy if-then rules [2]. Fractional calculus, as a field with practical implications, is applied in various domains such as economic processes [3], signal processing [4], chemical processes [5], and bioengineering [6]. In the last decade, fractional calculus was introduced in system theory and automated control [7]. Therefore, the application of fractional differential equations has resulted in more accurate dynamic system models, novel control strategies, and enhanced control loop characteristics, demonstrating fractional calculus's practical advantages and benefits.

In power electronics, converters are highly nonlinear and their control is crucial for industrial applications. DC-DC multilevel boost converters as high gain DC-DC sources are a key for advanced technology, simultaneously with the continuous advances in semiconductors and reactive components. Contrastly to the conventional DC-DC boost converter, the DC-DC multilevel boost converters can operate at a high-duty cycle to achieve a high output voltage, thus reducing switching frequency and decreasing electromagnetic interference [8]. Therefore, DC-DC multilevel converters can be used in many industrial domains, like automotive engineering, photovoltaic systems, and fuel cell applications [9]. Several DC-DC

multilevel boost converter (MBC) topologies were proposed in previous works [10]. They are similar to the conventional DC-DC boost converter by adding more capacitors and diodes. These topologies can generate a higher voltage at different levels by using only a single inductor and switch. The advantages of these configurations include the possibility of using switched capacitor converters without a transformer or a large duty cycle to achieve high voltage conversion ratios [11]. It is the best instance of the switched capacitor since the input current intensity is constant. The diodes have replaced all controlled switches in the switched capacitor mechanism [12].

This paper aims to establish a mathematical model for the tow-level boost converter (2-L MBC) based on the state-space averaged (SSA) method for developing the transfer functions of the input current and output voltage related to the duty cycle. Two control techniques are applied to 2-L MBC, the first is the fuzzy logic controller (FLC) and the second one is based on a fractional-order proportional-integral-derivative (FOPID) controller. The simulation results developed under MATLAB/Simulink and SimPowerSystems toolbox show that the dynamic responses with the proposed FOPID controller based on the Nelder-Mead optimization method are more accurate and faster than the ones obtained with the FLC controller.

2. MODELLING OF A REDUCED ORDER NONLINEAR DYNAMIC SYSTEM OF A 2-L MBC WITH EQUIVALENT CAPACITY

This section discusses the different steps in modeling the 2L-MBC based on the SSA method. The mathematical model of the 2L-MBC is non-linear. Although this system's nonlinearities mask, on average, all the information associated with the fast dynamics and instability of subharmonic oscillations, they are not captured [13]. Due to the multiplicative components linking the state variables to the duty cycle, the development of the mathematical model of the 2L-MBC is based on the SSA method in continuous conduction mode (CCM) [14], [15]. The input current and output voltage transfer functions are then developed and calculated. Figure 1 illustrates the power circuit of the 2L-MBC associated with the controller.

Steady-state and small signal modellings for a higher-order system are very complex. It is suitable to reduce the model for simplicity. However, considering the equivalent capacity during the switch-on and switch-off modes, applying the basic principles and considering that the capacitors are identical: $C_1=C_2=C_3=C$. In addition, the voltage across each capacitor is equal to the output voltage generated by N levels of capacitors. Where the state space vector is $x(t) = [I_L(t) \ V_C(t)]^t$ and the output $y(t)$ is the voltage load of the 2-L MBC which is noted by V_{Load} . There are two basic modes according to the state of the switch. The 2-L MBC can operate in different modes.

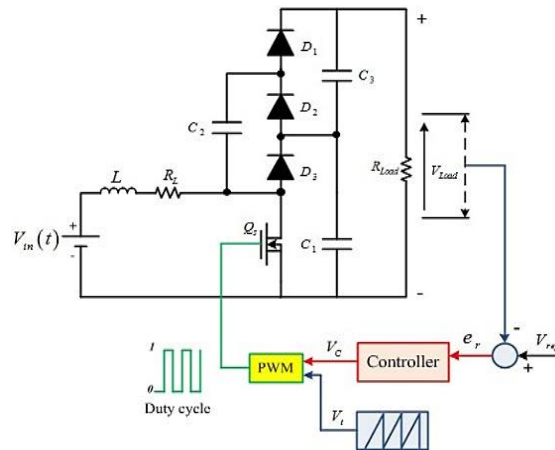


Figure 1. The power circuit diagram of the 2L-MBC controlled

2.1. Switch-on mode reduced order

The equivalent reduced order circuit in switch-on mode is depicted in Figure 2. The state space representation of the DC-DC 2-L MBC electrical model in switch-on mode is introduced by (1).

$$\begin{cases} \dot{x}(t) = A_1 x(t) + B_1 V_{in} \\ y(t) = C_1 x(t) \end{cases} \quad (1)$$

The matrix A_1 and the vectors B_1 and C_1 are presented by (2).

$$A_1 = \begin{bmatrix} -\frac{R_L}{L} & 0 \\ 0 & -\frac{N}{C_{eq1}R_{Load}} \end{bmatrix}; B_1 = \begin{bmatrix} \frac{1}{L} \\ 0 \end{bmatrix}; C_1 = [0 \quad 1] \quad (2)$$

2.2. Switch-off mode reduced order

Figure 3 illustrates the equivalent reduced order circuit in switch-off mode. The state space representation of the DC-DC 2-L MBC electrical model in switch-off mode is introduced by (3).

$$\begin{cases} \dot{x}(t) = A_2 x(t) + B_2 V_{in} \\ y(t) = C_2 x(t) \end{cases} \quad (3)$$

The matrix A_2 and the vectors B_2 and C_2 are presented by (4).

$$A_2 = \begin{bmatrix} -\frac{R_L}{L} & -\frac{1}{NL} \\ \frac{1}{C_{eq2}} & -\frac{1}{C_{eq2}R_{Load}} \end{bmatrix}; B_2 = \begin{bmatrix} \frac{1}{L} \\ 0 \end{bmatrix}; C_2 = [0 \quad 1] \quad (4)$$

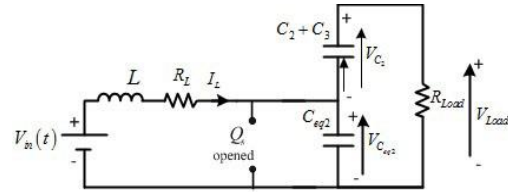
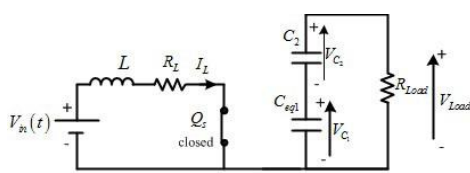


Figure 2. 2-L MBC switch-on mode reduced order

Figure 3. 2-L MBC switch-off mode reduced order

2.3. Nonlinear full-order dynamic model

To obtain the full-order dynamic model, the two operating mathematical models are combined into a single model by the mean of the SAA method presented by (5).

$$\begin{cases} A = A_1 d + A_2 (1 - d) \\ B = B_1 d + B_2 (1 - d) \end{cases}, \quad \begin{cases} C = C_1 d + C_2 (1 - d) \\ D = D_1 d + D_2 (1 - d) \end{cases} \quad (5)$$

A_1 , B_1 , C_1 , and D_1 are the state matrices in switch-on mode, whereas A_2 , B_2 , C_2 , and D_2 are the ones in switch-off mode. The average output voltage and current are expressed by (6) and (7) respectively:

$$V_{Load} = \left(\frac{N}{1-d} \right) V_{in} \quad (6)$$

$$I_{Load} = \left(\frac{1-d}{N} \right) I_L \quad (7)$$

Where N is the DC output link capacitor number; d : is the duty ratio; V_{in} : is the input voltage; By combining the from (1) to (5), the matrix system obtained by (8) and (9) represents the 2-L MBC mathematical model with the two switch modes.

$$\begin{bmatrix} \dot{I}_L(t) \\ \dot{V}_C(t) \end{bmatrix} = \begin{bmatrix} -\frac{R_L}{L} & -\frac{(1-d)}{NL} \\ \frac{(1-d)}{C_{eq}} & -\frac{1}{C_{eq}R_{Load}} \end{bmatrix} \begin{bmatrix} I_L(t) \\ V_C(t) \end{bmatrix} + \begin{bmatrix} \frac{1}{L} \\ 0 \end{bmatrix} V_{in} \quad (8)$$

$$[V_{Load}] = [0 \quad 1] \begin{bmatrix} I_L(t) \\ V_C(t) \end{bmatrix} \quad (9)$$

With the equivalent capacitor as given by (10).

$$dC_{eq1} + (1-d)C_{eq2} = C_{eq} \quad (10)$$

To establish the state space model, which is a combination of the two aforementioned operation models, the linearization of the system is done by (11).

$$X = [A_1 d + A_2(1 - d)]X + [B_1 d + B_2(1 - d)]U \quad (11)$$

2.4. State space averaging mathematical model of the 2-L MBC

The SSA method consists of introducing the term represented by ($\hat{\cdot}$) as a small perturbation. For instance, the variable $y(t)$ is written by (12):

$$y(t) = Y + \hat{y}(t) \quad (12)$$

Where Y is the DC term and \hat{y} is the small signal term. This approach is applied to the state space vector $x(t)$, the input voltage $v_{in}(t)$ and duty cycle $d(t)$. Applying the small perturbation approach to (11) which gives two expressions as given by (13). Therefore, two modes are obtained, AC and DC, expressed by (14) and (15) respectively.

$$\begin{aligned} \hat{x}_0 + \hat{x}(t) &= [A_1(D + \hat{d}) + A_2(1 - D - \hat{d})](x_0 + \hat{x}) + \\ &[B_1(D + \hat{d}) + B_2(1 - D - \hat{d})](u_0 + \hat{u}) \end{aligned} \quad (13)$$

- In DC mode

All the derivative terms are equal to zero, such as:

$$[A_1 D + A_2(1 - D)](x_0) + [B_1 D + B_2(1 - D)](u_0) = 0 \quad (14)$$

- In AC mode

Furthermore, in the AC equation, variables having products of \hat{x} , \hat{u} and \hat{d} are ignored (small variations multiplied by the same ones yields an even smaller result).

$$\begin{aligned} \hat{x}(t) &= [A_1 D + A_2(1 - D)]\hat{x}(t) + [B_1 D + B_2(1 - D)]\hat{u}(t) + \\ &[(A_1 - A_2)x_0 + (B_1 - B_2)u_0]\hat{d}(t) \end{aligned} \quad (15)$$

Where the capacitors $C_{eq2} = C$ and $C_{eq1} = 2C$ are replaced in (3) and (4), and taking into account that the DC-DC converter is two levels, thus $N = 2$ and $C_{eq} = C$. Consequently, the (15) is written in detailed form as given by (16).

$$\begin{bmatrix} \hat{x}_1(t) \\ \hat{x}_2(t) \end{bmatrix} = \begin{bmatrix} -\frac{R_L}{L} & -\frac{(1-D)}{2L} \\ \frac{(1-D)}{C} & -\frac{2}{CR_{Load}} \end{bmatrix} \begin{bmatrix} \hat{x}_1(t) \\ \hat{x}_2(t) \end{bmatrix} + \begin{bmatrix} \frac{1}{L} \\ 0 \end{bmatrix} \hat{u}(t) + \begin{bmatrix} 0 & \frac{1}{2L} \\ -\frac{1}{C} & \frac{1}{CR_{Load}} \end{bmatrix} \begin{bmatrix} x_{10} \\ x_{20} \end{bmatrix} \hat{d}(t) \quad (16)$$

2.5. Steady-state study

In order to deduce the solutions of x_{10} and x_{20} in a steady state, it is crucial to solve the system in DC continuous mode. The state of equilibrium is represented by (17).

$$\frac{dx}{dt} = Ax + Bu = 0 \Rightarrow \begin{bmatrix} 0 \\ 0 \end{bmatrix} = \begin{bmatrix} -\frac{R_L}{L} & -\frac{(1-D)}{2L} \\ \frac{(1-D)}{C} & -\frac{2}{CR_{Load}} \end{bmatrix} \begin{bmatrix} x_{10} \\ x_{20} \end{bmatrix} + \begin{bmatrix} \frac{1}{L} \\ 0 \end{bmatrix} V_{in} \quad (17)$$

The (18) and (19) introduce the current I_L and voltage V_C respectively which represent the DC values equivalent to x_{10} and x_{20} quantities, which are the solution of the (17).

$$I_L = \frac{4(1-D)}{4R_L(1-D) + R_{Load}(1-D)^3} V_{in} \quad (18)$$

$$V_C = \frac{2R_{Load}(1-D)}{4R_L + R_{Load}(1-D)^2} V_{in} \quad (19)$$

2.6. The transfer function of the DC-DC 2-L MBC

When the DC mode terms are omitted, the resulting matrix system presents the following small-signal model as given by (20).

$$\begin{bmatrix} \hat{i}_L(s) \\ \hat{v}_C(s) \end{bmatrix} = \begin{bmatrix} (Ls + R_L) & \frac{(1-D)}{2} \\ (1-D) & (-Cs - \frac{2}{R_{Load}}) \end{bmatrix}^{(-1)} * \begin{bmatrix} V_C \\ I_L \end{bmatrix} \hat{d}(s) + \begin{bmatrix} 1 \\ 0 \end{bmatrix} \hat{v}_{in}(s) \quad (20)$$

Following that, (21) and (22) present the current and voltage transfer functions, respectively.

$$\frac{\hat{i}_L(s)}{\hat{d}(s)} = \frac{\left(\frac{2(1-D)}{4R_L+(1-D)^2R_{Load}}V_{in}\right)\left(\left(Cs+\frac{2}{R_{Load}}\right)R_{Load}+1\right)}{CLs^2+\left(\frac{2L}{R_{Load}}+R_LC\right)s+\left(\frac{2R_L}{R_{Load}}+\frac{(1-D)^2}{2}\right)} \quad (21)$$

$$\frac{\hat{v}_C(s)}{\hat{d}(s)} = \frac{\left(\frac{V_{in}}{4R_L+(1-D)^2R_{Load}}\right)(-4(Ls+R_L)+2R_{Load}(1-D)^2)}{CLs^2+\left(\frac{2L}{R_{Load}}+R_LC\right)s+\left(\frac{2R_L}{R_{Load}}+\frac{(1-D)^2}{2}\right)} \quad (22)$$

3. CONTROL DESIGN

Two control methods are applied to the DC-DC 2-L MBC: the FLC and the FOPID. The two control strategies are compared with different tests.

3.1. Fuzzy logic controller design

The fuzzy logic controller's inputs are error and its derivative, and the output corresponds to the duty cycle variation, which are the most relevant quantities of the controller and are selected to improve control close to the desired operating point. Consequently, it requires a set of rules primarily determined by the operator's expertise when manipulating the system [16]. The characteristic parameters of the inputs of the FLC are denoted by (e) and (Δe) and output (Δd).

Figure 4 depicts the fuzzy logic block diagram, which is composed of the following four essential blocks. The normalization factors include those connected with the error and its variation and duty cycle variation. The fuzzification block converts input values to sub-fuzzy sets. The fuzzy inference mechanism block. The defuzzification block enables us to identify the actual output variable value from the fuzzy inference and convert it into a numerical value for application to the process.

a. Fuzzification

Membership functions (MFs) are used in this step to convert actual quantities into fuzzy variables. These MFs come in various forms, but triangular and trapezoidal are the most common. Figure 5 depicts the MFs of the input and output variables.

b. Fuzzy inference mechanism

The control output is generated by combining the (MFs) and control rules. The fuzzy control rules are a crucial element of this step, closely associated with human expertise. Depending on the Mamdani method [1], [17], 49 fuzzy rules of error and their variation are selected in Table 1.

c. Defuzzification

The defuzzification step uses the centroid method, which permits determining the output variable's actual value from the fuzzy inference mechanism [18]. This output value is then converted to a numerical value and applied to the process [19].

Table 1. Fuzzy rule base table for a duty cycle

Error (e)								
Variation of error (Δe)	NBe	NMe	NSe	Ze	PSe	PMe	PBe	
NB Δe	PB Δd	PB Δd	PB Δd	NB Δd	NM Δd	Z Δd	Z Δd	
NM Δe	PB Δd	PB Δd	PB Δd	PM Δd	PS Δd	Z Δd	Z Δd	
NS Δe	PB Δd	PM Δd	PS Δd	PS Δd	PS Δd	Z Δd	Z Δd	
Z Δe	PB Δd	PM Δd	PS Δd	Z Δd	NS Δd	NM Δd	NB Δd	
PB Δe	Z Δd	Z Δd	NM Δd	NS Δd	NS Δd	NM Δd	NB Δd	
NB Δe	Z Δd	Z Δd	NS Δd	NM Δd	NB Δd	NB Δd	NB Δd	
NB Δe	Z Δd	Z Δd	NM Δd	NB Δd	NB Δd	NB Δd	NB Δd	

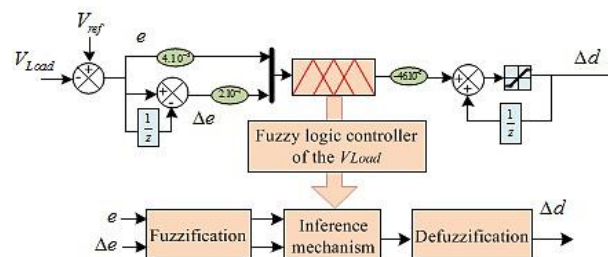


Figure 4. Block design of the FLC for DC-DC 2-L MBC output voltage control

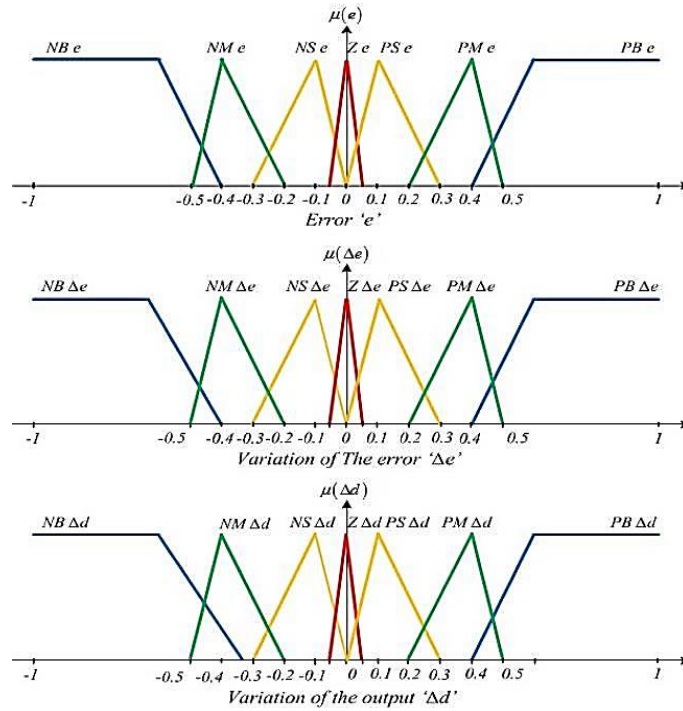


Figure 5. The MFs of the error (e), its variation (Δe) and the variation of the control (Δd)

3.2. Fundamental fractional calculus principles

The adaptation of differentiation and integration to non-integer order operators (${}_a\mathcal{D}_t^\alpha$) is referred to as fractional calculus so that the operation's bounds are (t) and (a), and a real number (α) denotes fractional order [20]. The fractional operator is established in several definitions. Considering Grünwald-Letnikov definition [21], [22]. This is one of the most used definitions to establish numerical solutions of the differential fractional order equations, and determined by (23).

$${}_a\mathcal{D}_t^\alpha f(t) = \frac{d_t^\alpha f(t)}{dt^\alpha} = \lim_{h \rightarrow 0} \frac{1}{h^\alpha} \sum_{k=0}^N (-1)^k \binom{\alpha}{k} f(t - kh) \quad (23)$$

The Laplace transform of the function's $f(t)$ α -th derivative with $\alpha \in \mathbb{R}_+$ and supposing the initial condition is zero at $t = 0$ is given by (24).

$$\ell\{{}_a\mathcal{D}_t^\alpha f(t)\} = s^\alpha F(s) = \frac{b_m s^{b_m} + b_{m-1} s^{b_{m-1}} + \dots + b_1 s^{b_1} + b_0 s^{b_0}}{a_n s^{a_n} + a_{n-1} s^{a_{n-1}} + \dots + a_1 s^{a_1} + a_0 s^{a_0}} \quad (24)$$

3.2.1. Fractional order 2L-MBC model identification

This section defines the identification of the fractional order model for the DC-DC 2L-MBC. The Oustaloup approximation filter method is used to represent the system dynamics efficiently and give a suitable fractional operator approximation for a specific frequency range [23]. Oustaloup filters approximate fractional operators efficiently described by the (25).

$$s^\alpha \approx K \prod_{k=-N}^N \frac{s + \omega'_k}{s + \omega_k} \quad (25)$$

ω'_k , ω_k and K are calculated using formulas given by (26):

$$\omega'_k = \left(\frac{b\omega_b}{b} \right)^{\frac{(\alpha+2k)}{2N+1}}; \quad \omega_k = \left(\frac{b\omega_h}{d} \right)^{\frac{(\alpha-2k)}{2N+1}}; \quad K = \omega_h^\alpha \quad (26)$$

N is the approximation order inside the frequency range $[\omega_b, \omega_h]$ and $\alpha \geq 1$, and taking into consideration, a good approximation is performed using the equation (26) with $b = 10$ and $d = 9$ [20]. The trust-region-reflective and Levenberg-Marquardt estimation techniques are used to find the integer order

system into a fractional order system, Assuming the variables y , u , and t are the identifying data structure stated by the MATLAB function: `iddata=fidata(y,u,t)` y represents the DC-DC 2L-MBC model output, u represents the input signal, and t represents the time vector. The coefficients are constrained in the interval $[10^2, 10^3]$, and the orders are bounded in the interval of $[10^{-9}, 5]$, and approximation within a frequency range of $[10^{-4}, 10^{+4}] \left(\frac{rad}{s}\right)$ using the Oustaloup filter, and the order of $N = 5$. The fractional order identification of the 2L-MBC system transfer function with the trust-region-reflective and Levenberg-Marquardt optimization algorithms are defined below, respectively by (27) and (28).

$$G_{TRR}(s) = \frac{(2.7645 \cdot \exp(5s^{0.93085}) + 514.18)}{(530.47s^{1.00000} + 551.83s^{0.87247} + 1)} \quad (27)$$

$$G_{LM}(s) = \frac{(8.9931s^{0.016868} + 239.62)}{(0.00091305s^{0.98128} - 0.027436s^{0.062356} + 1)} \quad (28)$$

A step response is utilized to compare the temporal domain properties of the derived models to those of the original model in Figure 6. The trust-region-reflective estimate approach yields a more precise result in this specific case. The time domain fit is excellent in both cases, but examining the temporal domain response reveals the distinct differences between the two models.

3.2.2. Fractional order PID controller (FOPID)

Podlubny was the first to introduce the notion of FOC in [24], [25]. The transfer function description of the FOPID controller is presented by expression (29):

$$G_{FO_PID}(s) = K_P + K_I s^{-\lambda} + K_D s^{\mu} \quad (29)$$

It is evident from (31) that the FOPID controller has five tuning parameters: a proportional gain (K_P), an integrator gain (K_I) with an order (λ) and a differentiator gain (K_D) with an order (μ). There are several FOPID design methods dependent on the controlled system. If the plant is represented by an integer-order model, conventional tuning techniques may be used to produce integer-order PID parameters. Then, FOPID orders may be adjusted to optimal performance. A tool is given that identifies the process (which may also be fractional-order) by using known models, which were studied in various previous scientific works [26].

MATLAB's FOMCON toolbox is designed to facilitate the creation of fractional-order models and controllers and evaluate their performance [27]. This study uses the FOPID controller to regulate the DC-DC 2L-MBC output voltage. The problem of optimizing parameters is resolved using the Nelder-Mead optimization criterion. Many studies discussed the convergence of the optimization with a family of functions of two variables. These studies emphasize on the necessity for variants of the original Nelder-Mead to guarantee the convergence problems [28]. The Nelder-Mead algorithm was improved for multidimensional, unconstrained optimization based on the selective simplex that allows the algorithm to choose its elements dynamically in contrast to the conventional Nelder-Mead algorithm, which uses a determinant simplex [29]. Another improvement of the algorithm, which uses a boosted incremental Nelder-Mead simplex algorithm, was applied to analyze a wireless sensor network by a distributed regression [30]. The Nelder-Mead simplex search was also used with the metaheuristic global optimization known as the state transition algorithm and the quadratic interpolation to enhance a local search [31]. The Nelder-Mead optimization can also be applied to the automatization and selective protection with the lowest tripping times by the minimization of an appropriately designed object function [32]. For higher dimensional problems, a multilevel methodology for a Nelder-Mead optimization was developed [33]. The methodology can enhance the optimizer's speed of convergence as it gets closer to the optimal solution.

The problem of optimizing parameters is resolved using the Nelder-Mead optimization criterion [34]. This is presented by Figure 7. Consider the trust-region-reflecting identification obtained model (27) from the integer model of the 2L-MBC. The FOMCON toolbox's (`fpid_optimize`) function gives a suboptimal FOPID for the 2L-MBC system under these conditions: $K_P = K_I = K_D = 1$, $\lambda = 0.9$ and $\mu = 0.7$. The proportional and integral, and derivative gains are defined by the search limits: $[K_P, K_I, K_D] \in [0, 100]$. The Oustaloup filter approximation is used for simulation with default settings that $\omega \in [10^{-4}, 10^{+5}] \left(\frac{rad}{s}\right)$ and an order $N = 10$. The specifications are shown as: The gain margin is 10 dB, and the phase margin is 45 degrees. Integral absolute error (IAE) as given by (30), is used as a performance metric to minimize the overshoot and the settling time in the closed-loop response of the system.

$$IAE = \int_0^t |e_r(t)| dt \quad (30)$$

Then, the necessity for robustness to gain changes is imposed, together with the recovery of the crossover frequency ω_c , which is calculated by (31).

$$\left. \frac{d \arg(F(j\omega))}{d\omega} \right|_{\omega=\omega_c} = 0 \quad (31)$$

Where $F(j\omega)$ is the open-loop frequency response of the DC-DC 2L-MBC system and FOPID controller. Moreover, to avoid gain fluctuation, the phase response at critical frequency must be flat. After 631 repeated iterations of the Nelder-Mead algorithm, the suboptimal FOPID controller settings are computed as given by (32).

$$\begin{cases} K_P = 0.013775 & K_I = 0.0024307 \\ K_D = 0.01494 & \lambda = 0.50021 \\ \mu = 0.0334 \end{cases} \quad (32)$$

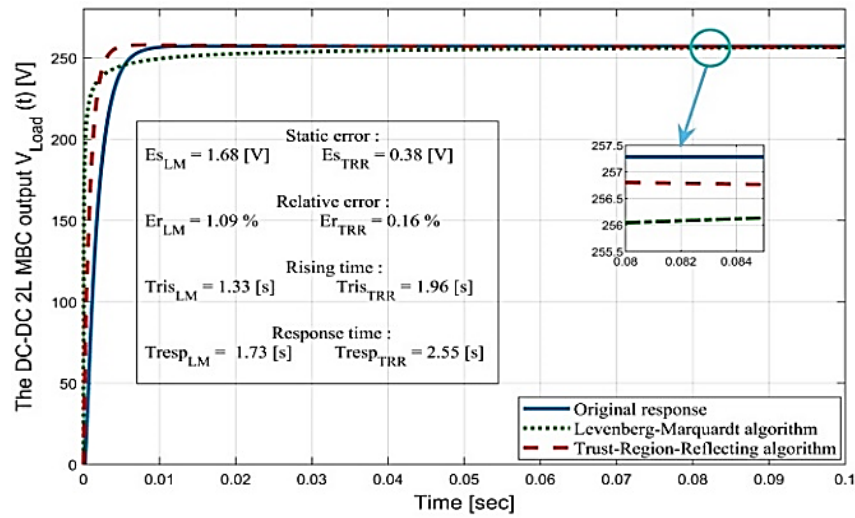


Figure 6. Step responses of identified and original models

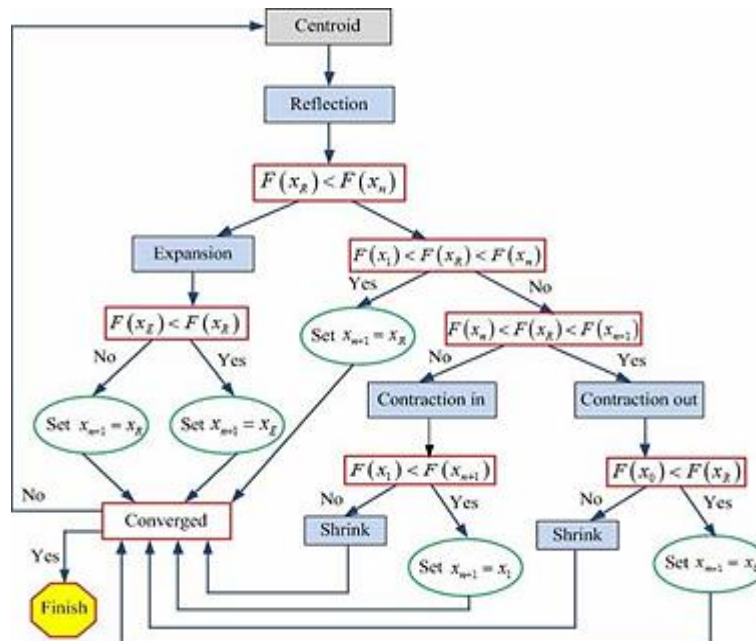


Figure 7. Nelder-Mead flowchart to tune the parameters of the FOPID controller

4. SIMULATION AND RESULTS

To evaluate the performance of the FLC and FOPID controllers using a VMC control approach of the DC-DC 2L-MBC, a program was implemented under MATLAB/Simulink to achieve a set of simulation tests. The system's simulation parameters are given in the Table 2. Figures 8 and 9 show the duty cycle, input current, and output voltage of the 2L-MBC using FLC and FOPID controllers. Rapid step changes are applied to the reference voltage, starting with 100 (V) from 0 to 0.07 s, 80 (V) from 0.07 to 0.14 s, and ending with 120 (V) from 0.14 to 0.2 s.

Figures 10 and 11 depict input current and output voltage using FLC and FOPID controllers to evaluate the efficiency of the proposed controllers. First, the system is initially supplied with an input voltage of 50 volts, then a step change from 50 to 40 volts is applied at $t=0.07$ s, succeeded by a step change from 40 to 60 volts at $t=0.14$ s. Finally, Figures 12 and 13 analyze and show an essential aspect of the controller's operation: the system's response to load changes. At $t=0.07$ s, the load resistor is dropped from its nominal value of 10 (Ω) to 6 (Ω) and subsequently raised from 6 (Ω) to 16 (Ω) at $t=0.14$ s. The simulation results demonstrate that the voltage drop is recovered more rapidly by the FOPID controller than by the FLC when a sudden change in load occurs.

Table. 2 Simulation parameters		
The DC-DC two-level boost converter parameters		
Parameters	Variables	Values
Input voltage	V_{in}	50 [V]
Duty cycle	D	0.5
Output voltage	V_o	200 [V]
Inductor	L	100 [μH]
Inductor resistance	R_L	0.0516 [Ω]
Capacitor	C	200 [μF]
Load resistor	R_{Load}	10 [Ω]
Switching frequency	F_s	25 [Khz]
Sampling time	T_s	1 [μs]

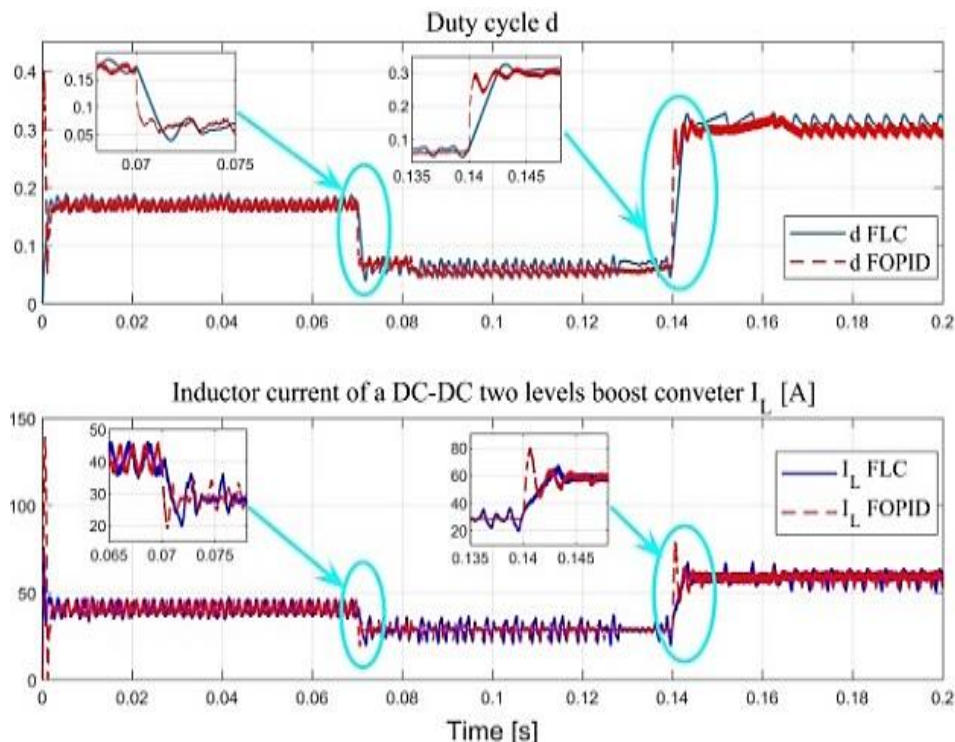


Figure 8. Duty cycle and inductor current of the DC-DC 2-L MBC with change in reference voltage (100, 80, and 120 volts) using FLC and FOPID

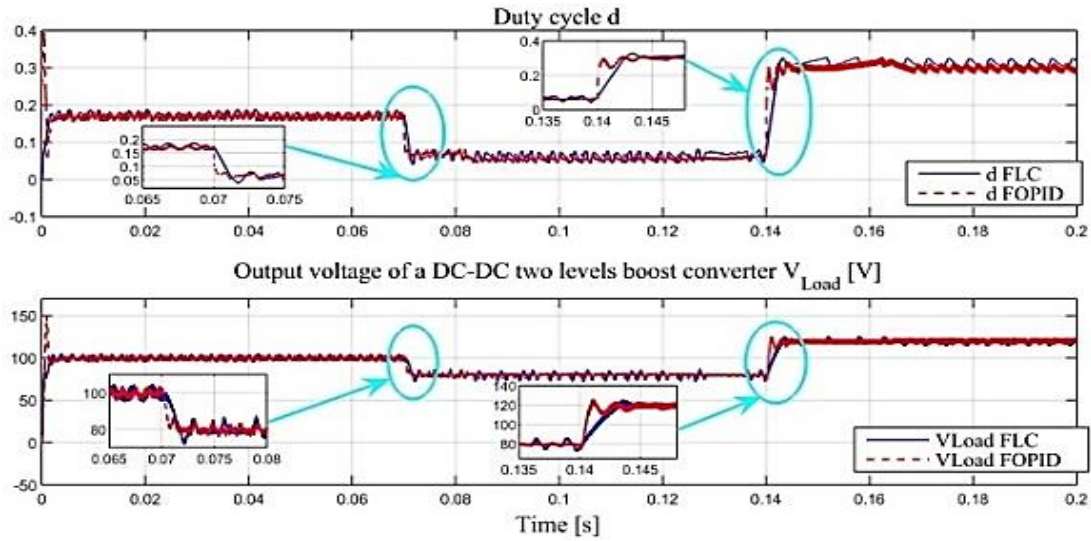


Figure 9. Duty cycle and output voltage of the DC-DC 2-L MBC with change in reference voltage (100, 80, and 120 volts) using FLC and FOPID

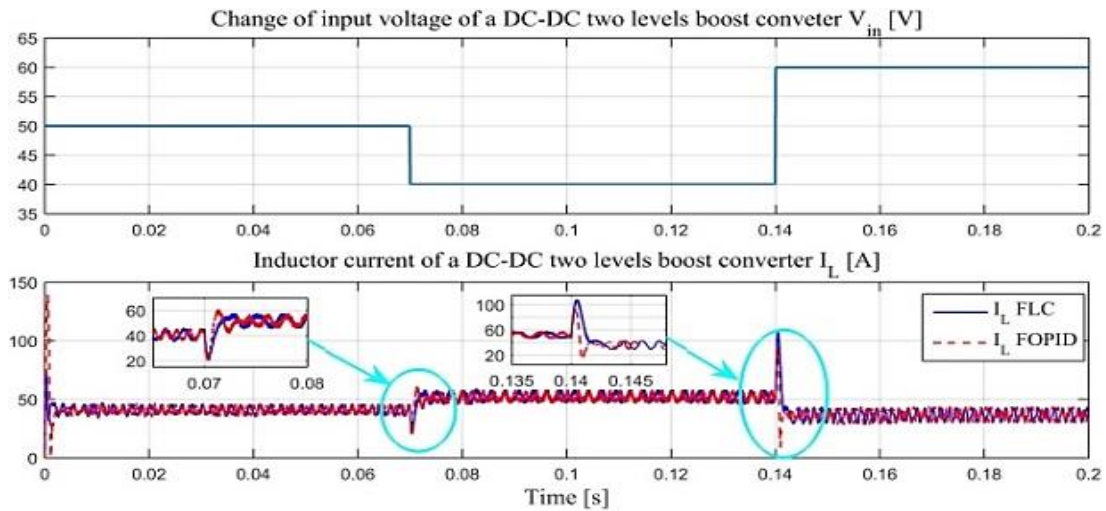


Figure 10. Inductor current of the DC-DC 2-L MBC with change in the input voltage using FLC and FOPID

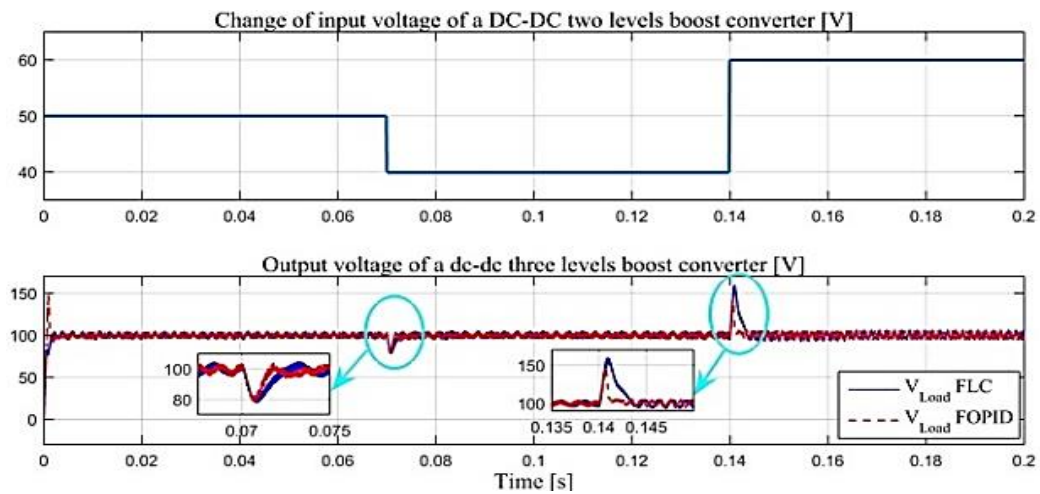


Figure 11. Output voltage of the DC-DC 2-L MBC with change in the input voltage using FLC and FOPID

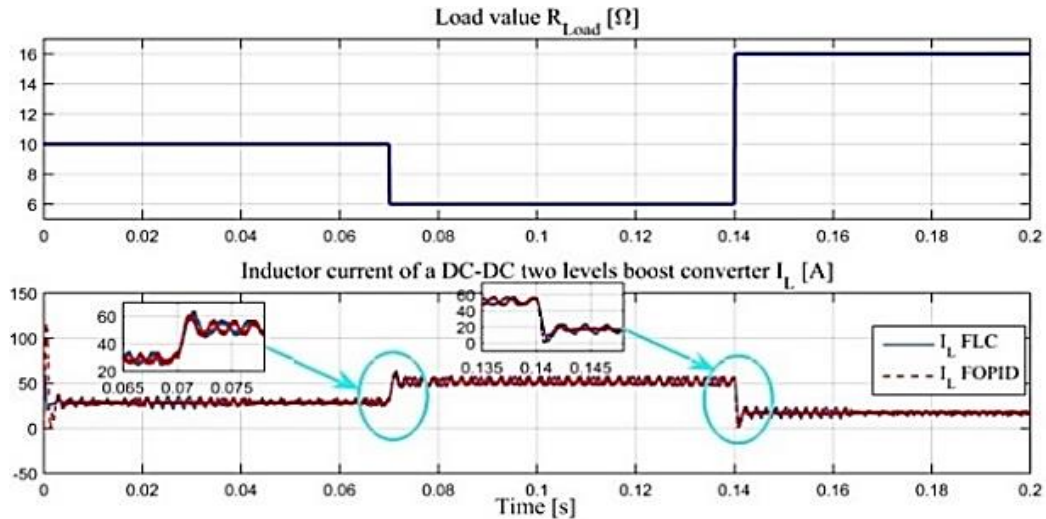


Figure 12. Inductor current of the DC-DC 2-L MBC with change in the load resistor using FLC and FOPID

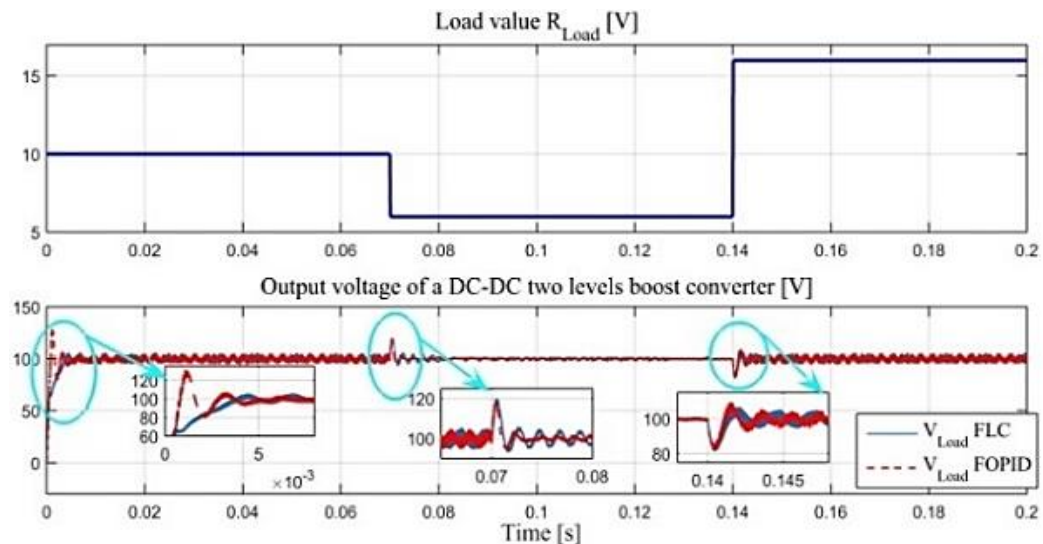


Figure 13. The output voltage of the DC-DC 2-L MBC with change in the load resistor using FLC and FOPID

5. CONCLUSION




This study compares and analyzes two control methods, FLC and FOPID controller, applied to the DC-DC 2L-MBC converter in VMC mode operation. The optimization process to evaluate the performance of the FOPID controller is done using the Nelder Mead optimization method and applied to the DC-DC 2L-MBC converter mathematical model obtained using the SSA method. The simulation results show that the FOPID controller has better dynamic performance than the FLC controller. The FOPID controller can effectively track the reference signals and maintain the output voltage of the 2L-MBC DC-DC converter at the setpoint with minimal deviation. Moreover, the FOPID controller offers a significantly faster start-up response and better dynamic reaction across the entire control range than the FLC controller. The MATLAB-Simulink simulations have shown that the 2L-MBC controlled by the non-conventional controller as FOPID has higher dynamic performance with reduced settling time and a minimal overshoot than the FLC control.

REFERENCE




- [1] E. H. Mamdani and S. Assilian, "An experiment in linguistic synthesis with a fuzzy logic controller," *International Journal of Man-Machine Studies*, vol. 7, no. 1, pp. 1-13, 1975, doi: 10.1016/S0020-7373(75)80002-2.
- [2] N. Wakami, S. Araki, and H. Nomura, "Recent applications of fuzzy logic to home appliances," in *Proceedings of IECON'93-19th Annual Conference of IEEE Industrial Electronics*, 1993, pp. 155-160, doi: 10.1109/IECON.1993.339089.

- [3] A. W. Lo, "Long-term memory in stock market prices," *Econometrica: Journal of The Econometric Society*, vol. 59, no. 5, pp. 1279-1313, 1991, doi: 10.2307/2938368.
- [4] B. M. Vinagre, Y. Q. Chen, and I. Petráš, "Two direct Tustin discretization methods for fractional-order differentiator/integrator," *Journal of the Franklin Institute*, vol. 340, no. 5, pp. 349-362, 2003, doi: 10.1016/j.jfranklin.2003.08.001.
- [5] K. Oldham and J. Spanier, *The fractional calculus theory and applications of differentiation and integration to arbitrary order*. Amsterdam: Elsevier, 1974.
- [6] C. M. Ionescu, *The human respiratory system: an analysis of the interplay between anatomy, structure, breathing and fractal dynamics*. London: Springer Science & Business Media, 2013, doi: 10.1007/978-1-4471-5388-7.
- [7] Z. Li, L. Liu, S. Dehghan, Y. Chen, and D. Xue, "A review and evaluation of numerical tools for fractional calculus and fractional order controls," *International Journal of Control*, vol. 90, no. 6, pp. 1165-1181, 2017, doi: 10.1080/00207179.2015.1124290.
- [8] M. Meraj, M. S. Bhaskar, A. Iqbal, N. Al-Emadi, and S. Rahman, "Interleaved multilevel boost converter with minimal voltage multiplier components for high-voltage step-up applications," *IEEE Transactions on Power Electronics*, vol. 35, no. 12, pp. 12816-12833, 2020, doi: 10.1109/TPEL.2020.2992602.
- [9] K. A. Mahafzah and H. A. Rababah, "A novel step-up/step-down DC-DC converter based on flyback and SEPIC topologies with improved voltage gain," *International Journal of Power Electronics and Drive Systems (IJPEDS)*, vol. 14, pp. 898-908, 2023, doi: 10.11591/ijpeds.v14.i2.pp898-908.
- [10] L. Piansangsan and S. Pattanasethanon, "A Voltage-Lift Switched Inductor DC/DC Multilevel Boost Converter," *Przegląd Elektrotechniczny*, vol. 91, pp. 127-130, 2015, doi: 10.15199/48.2015.04.28.
- [11] E. Durán, S. P. Litrán, and M. Bella Ferrera, "Configurations of DC-DC converters of one input and multiple outputs without transformer," *IET Power Electronics*, vol. 13, no. 12, pp. 2658-2670, 2020, doi: 10.1049/iet-pel.2019.1251.
- [12] K. Mahalingam and G. Jothamani, "An elevated gain DC-DC converter with active switched inductor for PV application," *International Journal of Power Electronics and Drive Systems (IJPEDS)*, vol. 14, no. 2, pp. 892-897, 2023, doi: 10.11591/ijpeds.v14.i2.pp892-897.
- [13] A. S. Samosir, T. Sutikno, and L. Mardiyah, "Simple formula for designing the PID controller of a DC-DC buck converter," *International Journal of Power Electronics and Drive Systems*, vol. 14, no. 1, p. 327, 2023, doi: 10.11591/ijpeds.v14.i1.pp327-336.
- [14] Z. Wang, K. Xu, Y. Lan, and X. Yang, "Novel Explicit Model Predictive Control Strategy For Boost Converters Based on State-space Averaging Method," in *IECON 2022-48th Annual Conference of the IEEE Industrial Electronics Society*, 2022, pp. 1-8, doi: 10.1109/IECON49645.2022.9968518.
- [15] F. Tahri, A. Tahri, A. Allali, and S. Flazi, "The digital self-tuning control of step a down DC-DC converter," *Acta Polytechnica Hungarica*, vol. 9, no. 6, pp. 49-64, 2012.
- [16] C. Napole, M. Derbeli, and O. Barambones, "Experimental validation of fuzzy type-2 against type-1 scheme applied in DC/DC converter integrated to a PEM fuel cell system," *Energy Science & Engineering*, vol. 14, no. 1, 2022, doi: 10.1002/ese3.1355.
- [17] M. Nagaiah and K. C. Sekhar, "Analysis of fuzzy logic controller based bi-directional DC-DC converter for battery energy management in hybrid solar/wind micro grid system," *International Journal of Electrical and Computer Engineering*, vol. 10, no. 3, pp. 2271-2284, 2020, doi: 10.11591/ijece.v10i3.pp2271-2284.
- [18] M. H. Azmi, S. Z. M. Noor, and S. Musa, "Fuzzy logic control based maximum power point tracking technique in standalone photovoltaic system," *International Journal of Power Electronics and Drive Systems (IJPEDS)*, vol. 14, no. 2, pp. 1110-1120, 2023, doi: 10.11591/ijpeds.v14.i2.pp1110-1120.
- [19] G. Tahri, Z. A. Foitih, and A. Tahri, "Fuzzy logic control of active and reactive power for a grid-connected photovoltaic system using a three-level neutral-point-clamped inverter," *International Journal of Power Electronics and Drive Systems*, vol. 12, no. 1, pp. 453-462, 2021, doi: 10.11591/ijpeds.v12.i1.pp453-462.
- [20] K. Bingi, R. Ibrahim, M. N. Karsiti, S. M. Hassan, and V. R. Harindran, *Fractional-order systems and PID controllers*. Cham: Springer Nature, 2020.
- [21] B. Wang, S. Wang, Y. Peng, Y. Pi, and Y. Luo, "Design and high-order precision numerical implementation of fractional-order PI controller for PMSM speed system based on FPGA," *Fractal and Fractional*, vol. 6, no. 4, 2022, doi: 10.3390/fractalfract6040218.
- [22] Y. Marushchak and B. Kopchak, "Information support of controlling influences formation using fractional order controllers," in *ITEA-2021*, 2022.
- [23] A. Oustaloup, F. Levron, B. Mathieu, and F. M. Nanot, "Frequency-band complex noninteger differentiator: characterization and synthesis," *IEEE Transactions on Circuits and Systems I: Fundamental Theory and Applications*, vol. 47, no. 1, pp. 25-39, 2000, doi: 10.1109/81.817385.
- [24] I. Podlubny, "Fractional-order systems and PI/sup/spl lambda//D/sup/spl mu//-controllers," *IEEE Transactions on automatic control*, vol. 44, no. 1, pp. 208-214, 1999, doi: 10.1109/9.739144.
- [25] I. Podlubny, L. Dorcak, and I. Kostial, "On fractional derivatives, fractional-order dynamic systems and PI/sup/spl lambda//D/sup/spl mu//-controllers," in *Proceedings of the 36th IEEE Conference on Decision and Control*, 1997, pp. 4985-4990, doi: 10.1109/CDC.1997.649841.
- [26] D. Horla and T. Sadalla, "Optimal tuning of fractional-order controllers based on Fibonacci-search method," *ISA transactions*, vol. 104, pp. 287-298, 2020, doi: 10.1016/j.isatra.2020.05.022.
- [27] A. Tepljakov, *Fractional-order modeling and control of dynamic systems*. Cham: Springer, 2017, doi: 10.1007/978-3-319-52950-9.
- [28] K. I. McKinnon, "Convergence of the Nelder-Mead Simplex method to a nonstationary Point," *SIAM Journal on optimization*, vol. 9, no. 1, pp. 148-158, 1998, doi: 10.1137/S1052623496303482.
- [29] H. A. MUSAFAER and A. MAHMOOD, "Dynamic hassan nelder mead with simplex free selectivity for unconstrained optimization," *IEEE Access*, vol. 6, pp. 39015-39026, 2018, doi: 10.1109/ACCESS.2018.2855079.
- [30] P. J. Marandi and N. M. Charkari, "Boosting Incremental Nelder-Mead Simplex for Distributed Regression over Wireless Sensor Networks" in *2008 International Symposium on Telecommunications*, 2008, doi: 10.1109/ISTEL.2008.4651397.
- [31] L. Zhou, X. Zhou, and C. Yi, "A Hybrid STA Based on Nelder-Mead Simplex Search and Quadratic Interpolation," *Electronics*, vol. 12, no. 4, p. 994, 2023, doi: 10.3390/electronics12040994.
- [32] J. Ehrenberger and J. Švec, "Nelder Mead method used in protection setting optimization," in *2016 17th International Scientific Conference on Electric Power Engineering (EPE)*, 2016, pp. 1-6, doi: 10.1109/EPE.2016.7521806.
- [33] G. S. Kumar and V. Suri, "Multilevel Neider Mead's simplex method," in *2014 9th International Conference on Industrial and Information Systems (ICIIS)*, 2014, pp. 1-6, doi: 10.1109/ICIINFS.2014.7036549.
- [34] J. C. Lagarias, J. A. Reeds, M. H. Wright, and P. E. Wright, "Convergence properties of the Nelder-Mead simplex method in low dimensions," *SIAM Journal on optimization*, vol. 9, no. 1, pp. 112-147, 1998.




BIOGRAPHIES OF AUTHORS

Ghrissi Tahri    was born in Oran, Algeria, in Jun 1984. He received the ingéniorat d'état in control engineering from the University of Sciences and Technology of Oran (USTO-MB), Algeria, in 2007. He received his magister degree in Electronics Engineering, option: Automatic-Robotic-Productic, from USTO-MB University in 2011. He got the Ph.D. degree in Electronics Engineering, option: Control Engineering, at USTO-MB in 2022. Moreover, he is an associate professor at the Department of Applied Physics and Optics at the Institut des Sciences et Techniques Appliquées (ISTA), University Oran 1, Oran, Algeria. His research interests include control systems, power electronics and renewable energy systems. He is also a member of the Electrical Engineering Laboratory of Oran LGEO at USTO-MB University. He can be contacted at email: ghrissi@univ-oran1.dz or ghrissi.tahri@univ-usto.dz.



Fatima Tahri    was born in Mers El Kebir in Oran, Algeria, in August 1978. She received the ingéniorat d'état, the M.Sc and Ph.D. degrees from the University of Sciences and Technology of Oran (USTO-MB), Algeria, in 2002, 2006, and 2014, respectively, all in Electrical Engineering. Her main research interests are power electronics, DC-DC converters, advanced static var compensation systems, and photovoltaic systems. She is now an assistant professor at the Higher School of Electrical and Energetic Engineering of Oran, ESGEE, Algeria and a member of the Electrical Engineering Laboratory of Oran LGEO and the Laboratory of Smart Grid Development. She can be contacted at email: fatimatahri.dz@gmail.com.



Ali Tahri    is a full professor at the Electrical Engineering Faculty in the University of Science and Technology of Oran (USTO), Algeria. He received the ingeniorat d'état, the M.Sc. and the Ph.D. degrees from the USTO in 1992, 1997, and 2006 respectively all in Electrical Engineering. His main research interests are in the field of analysis, modelling and simulation of power converters, the advanced static VAR compensation and FACTS systems, embedded systems and photovoltaic systems. He has co-authored in several book chapters. He is now a member of the Electrical Engineering Laboratory of Oran LGEO. He can be contacted at email: ali.tahri@univ-usto.dz.